https://doi.org/10.1016/j.jpowsour.2017.10.049

A membrane electrode assembled photoelectrochemical cell with a solar-responsive mesoporous CdS-ZnS-TiO_2/SBA-15 photoanode

Ming Chen[1,2], Rong Chen[1,2*], Xun Zhu[1,2*], Qiang Liao[1,2], Liang An[3*], Dingding Ye[1,2], Yuan Zhou[1,2], Xuefeng He[1,2], Wei Zhang[1,2]

[1]Key Laboratory of Low-grade Energy Utilization Technologies and Systems, Chongqing University, Ministry of Education, Chongqing 400030, P.R. China

[2]Institute of Engineering Thermophysics, Chongqing University, Chongqing 400030, P.R. China

[3]Department of Mechanical Engineering, The Hong Kong Polytechnic University, Hung Hom, Kowloon, Hong Kong, China

*Corresponding authors:

[1,2] Tel.: 0086-23-65102019; fax: 0086-23-65102474; e-mail: rchen@cqu.edu.cn (Rong Chen)

[1,2] Tel.: 0086-23-65102474; fax: 0086-23-65102474; e-mail: zhuxun@cqu.edu.cn (Xun Zhu)

[3] Tel.: Tel.: 852-27667820; fax: 852-23654703; e-mail: liang.an@polyu.edu.hk (Liang An)

Abstract

In this work, a membrane electrode assembled photoelectrochemical cell (PEC) is developed for the electricity generation by degrading the organic compounds. The photocatalyst is prepared by the incorporation of mesoporous SBA-15 and the photosensitization of CdS-ZnS to enhance the photoanode performance, while the cathode employs the air-breathing mode to enhance the oxygen transport. The experimental results show that the developed PEC exhibits good photoresponse to the illumination and the appropriate SBA-15 mass ratio in the photoanode enables the enhancement of the performance. It is also shown that the developed PEC yields better performance in the alkaline environment than that in the neutral environment.

Increasing the KOH concentration can improve the cell performance. There exist optimal liquid flow rate and organics concentration leading to the best performance. Besides, it is found that increasing the light intensity can generate more electron-hole pairs and thus enhance the cell performance. These results are helpful for optimizing the design.

***Keywords*:** Photoelectrochemical cell; Membrane electrode assembly; Mesoporous silica; Air-breathing cathode; Cell performance

1. Introduction

Each year, a significant quantity of wastewater that contains abundant chemical energy is discharged into water body, causing severe water pollution and threatening the human health [1]. To resolve this challenging issue, several wastewater treatment technologies have been developed, such as the cavitation [2], photocatalytic oxidation [3], photocatalytic ozonation [4], Fenton's chemistry ozonation [5] and so on [6]. However, these technologies mainly focus on the efficiency and velocity of degrading organic compounds, leading to a large amount of energy to be wasted [7, 8]. Hence, recovering the potential chemical energy stored in wastewater and turning it into a useful energy form are essential to simultaneously alleviate the environmental and energy problems. Photoelectrochemical cell (PEC) is one of such kind technologies to meet this demand [9]. Upon illumination, the degradation of a variety of organic pollutants into nontoxic materials and electricity generation can be realized simultaneously [10]. Because of this feature, the PEC has become an increasing-attention research field [11].

Previous studies on the PEC mainly focused on the development of highly-efficient photoanode catalysts [12-14]. For instance, Liu et al. [12] developed the photocatalytic fuel cell (PFC) with a TiO_2-nanotube-array-based photoanode to use refractory organic compounds as substrates for electricity generation, which was also a typical PEC system. Antoniadou et al. [13] developed the visible-light responsive photocatalyst by adding CdS-ZnS for water splitting in the presence of sacrificial agents. Although significant progress on the photoanode catalyst has been made, the

performance of existing photoanode is still limited by low specific surface area [15]. Hence, mesoporous materials with large specific surface area and pore volume have been incorporated into the photocatalysts to increase the specific surface area, the dispersion of nanoparticles, and the photocatalytic activity [16, 17]. In addition to the photoanode catalysts, the performance of the PEC is also greatly influenced by the reactor design. Traditional PECs usually employ single-compartment and double-compartment designs [11, 18]. For single-compartment PEC, the mixture of organics and electrolyte is supplied to the electrodes [19, 20], so that the organics reaching to the cathode can form the mixed potential and thus lower the cathode performance [21]. For double-compartment PEC, the photoanode and cathode are separated by an ion exchange membrane [22, 23], in which large distance between the electrodes causes the problems of large ion transfer resistance and gross structure. Moreover, the oxygen required by the cathodic reactions usually comes from the oxygen dissolved electrolyte [24]. In this case, not only the oxygen transport is limited due to low solubility of oxygen but also the ancillary devices for the oxygen supply are required. To enhance the oxygen transport and eliminate ancillary devices associated with the oxygen supply, Li et al. [25] developed a micro PFC with an air-breathing cathode to replace the oxygen dissolved cathode.

Membrane electrode assembly (MEA), in which the anode, membrane and cathode are sandwiched together by hot-press, has been widely employed in conventional fuel cells [26, 27]. The utilization of the MEA can make the fuel cell system more compact and flexible. Using the MEA design, Seger and Kamat used the TiO_2

photoanode to replace Pt and developed a MEA based photoelectrochemical cell to generate the photocurrent and hydrogen under UV irradiation [28]. However, this photoanode could only respond to the UV light and had low specific surface area, limiting the improvement in the photoelectrochemical reactions. Hence, we proposed a membrane electrode assembled photoelectrochemical cell in this work to simultaneously degrade the organics and generate electricity upon the visible light irradiation. The photoanode was formed via incorporating mesoporous material (silica, SBA-15) into the TiO_2 followed by the quantum-dot-sensitization of CdS-ZnS, termed as CdS-ZnS-TiO_2/SBA-15. This photoanode could not only respond to the visible light but also have large specific surface area and pore volume, thereby improving the photocatalytic activity and mass transport efficiency. The air-breathing cathode was employed to enhance the oxygen transport and simplify the PFC system. The performance of the developed PEC with the MEA design was accessed by using ethanol as a model organic pollutant under various conditions.

2. Experimental

2.1 Construction of photoanode

The composite photoanode of CdS-ZnS-TiO_2/SBA-15 was prepared by the following three steps: the preparation of the TiO_2/SBA-15 colloid, the construction of the TiO_2/SBA-15 film on the carbon paper (Toray 090, Japan) and the quantum-dot sensitization by CdS-ZnS. In the first step, the TiO_2/SBA-15 colloid was prepared by the sol-gel method [29]. Here, a given amount of TiO_2 nanoparticles (Aeroxide P25, Acros, Belgium) and a given amount of SBA-15 particles (Nathmay, China) were put

into an agate mortar and grinded for 5 minutes to make them uniformly mixed. The mixed powders were then added into the mixture of 120 mL deionized water and 0.4 mL acetylacetone (Sigma-Aldrich, USA) with magnetic stirring. After that, 0.2 mL Triton X-100 (Sigma-Aldrich, USA) was added to facilitate the spreading of the colloid. Finally, 2.4 g polyethylene glycol (Aladdin, China) was added into the solution and magnetically stirred for 12 hours. In the second step, the carbon paper was cut into the size of 2.0 cm × 2.2 cm and ultrasonically cleaned in deionized water for 10 min. After drying, an adhesive tape was used to cover one edge of the carbon paper, forming an exposed area of 2.0 cm × 2.0 cm for coating TiO_2/SBA-15. Then the TiO_2/SBA-15 colloid was sprayed on the exposed carbon paper by a spray gun until the total photocatalyst loading of TiO_2/SBA-15 was about 3 mg/cm^2. The loading was determined by the mass difference between the carbon papers without/with the coated photocatalysts over the active area of the electrode. During the spray process, the mass of the carbon paper with the coated photocatalysts was frequently measured until the target loading was achieved. After that, the adhesive tape was removed and the photocatalysts coated carbon paper underwent the calcination at 550 ℃ for 2 h. In this work, we prepared four photoanodes with various SBA-15 mass ratios defined as the ratio of the SBA-15 mass to the TiO_2 mass, The SBA-15 ratio ranged from 15%, 30%, 45% to 60%, which were represented by CdS-ZnS-TiO_2/15% SBA-15, CdS-ZnS-TiO_2/30% SBA-15, CdS-ZnS-TiO_2/45% SBA-15 and CdS-ZnS-TiO_2/60% SBA-15, respectively. The third step aimed to form the CdS-ZnS composite on TiO_2/SBA-15 film by successive ionic layer adsorption

and reaction (SILAR) [30]. Two aqueous solutions were prepared, one containing $Cd(NO_3)_2 \cdot 4H_2O$ (Aladdin, China) and $Zn(NO_3)_2 \cdot 6H_2O$ (Aladdin, China) with a molar ratio of 3 and the other one containing $Na_2S \cdot 9H_2O$ (Aladdin, China). The concentration of metal ions as well as the concentration of sulfur ions were 0.1 M. The TiO_2/SBA-15 coated carbon paper was put into the $Cd(NO_3)_2$ and $Zn(NO_3)_2$ mixed solution for 4 minutes and then washed in deionized water. After that, it was put into the $Na_2S \cdot 9H_2O$ solution for 4 minutes and washed in deionized water again. This sequence corresponded to one SILAR cycle. 4 SILAR cycles were repeated and then dried with N_2 stream. Finally, the CdS-ZnS-TiO_2/SBA-15 coated carbon paper was put into an oven at 100 ℃ for 10 minutes. It was found that the prepared photoanode showed yellow color because of the quantum-dot-sensitization by CdS-ZnS, indicating that the visible-light responsive photoanode has been successfully prepared.

2.2 Construction of cathode

The cathode was made of the carbon black coated carbon paper (HCP120, Hesen, China) with deposited Pt black (JM, Hesen, China). The cathode was prepared by the following three steps. First, 0.1 g Pt black electrocatalyst was mixed with 2.5 g distilled water. Then 2.5 g isopropanol (Aladdin, China) and 0.5 g Nafion® perfluorinated resin (D520, 5% wt. DuPont Co. USA) were added. The prepared mixture was then applied on the carbon black coated carbon paper (2.0 cm × 2.0 cm) by a spray gun. Subsequently, the electrode was heated at 80 °C for 30 minutes. The Pt loading was about 1 mg/cm^2.

2.3 Assembly of membrane and electrodes

Before the MEA fabrication, 5% Nafion® perfluorinated resin solution was firstly sprayed onto the surface of the prepared cathode. To do this, 0.4 mg Nafion® solution was sprayed onto the side of the cathode with catalysts. After that, the ionomer coated cathode with the catalyst coated side toward the membrane was hot-pressed with the Nafion® membrane (211, Hesen, China) at 0.5 MPa and 135 ℃ for 3 min. Subsequently, the photoanode was directly attached to the other side of the Nafion® membrane without hot-pressed, forming a membrane electrode assembly with the active area of 2.0 cm × 2.0 cm=4 cm^2.

2.4 PEC fixture

As shown in Fig. 1a, the fabricated MEA was sandwiched between two electrical current collectors. A serpentine flow field was drilled in the both current collectors, which served as the passages of light, solution and oxygen. The PEC was held together between a photoanode fixture and a cathode fixture, both of which were made of transparent PMMA plates. In this work, the stainless steel plate with the thickness of 1 mm was used to fabricate the current collectors because the stainless steel had good electric conductivity and mechanical strength and was easy for fabrication. The serpentine flow field with the width of 1 mm was formed by laser cutting and the rib size was 1.15 mm, resulting in an open ratio of 0.5. In the center of the cathode PMMA fixture, a 2.0 cm × 2.0 cm hole was drilled for breathing oxygen from air. Finally, the prepared MEA, the photoanode and cathode current collectors

and fixtures were assembled by eight bolts. The fabricated PEC with the MEA design is shown in Fig. 1b.

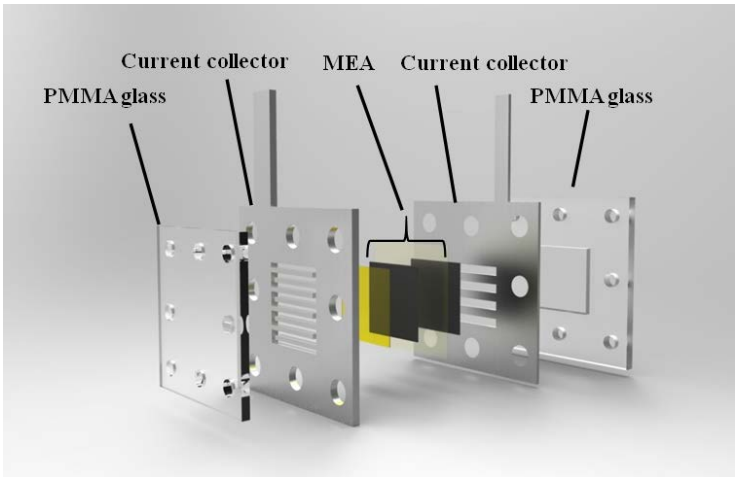

(a)

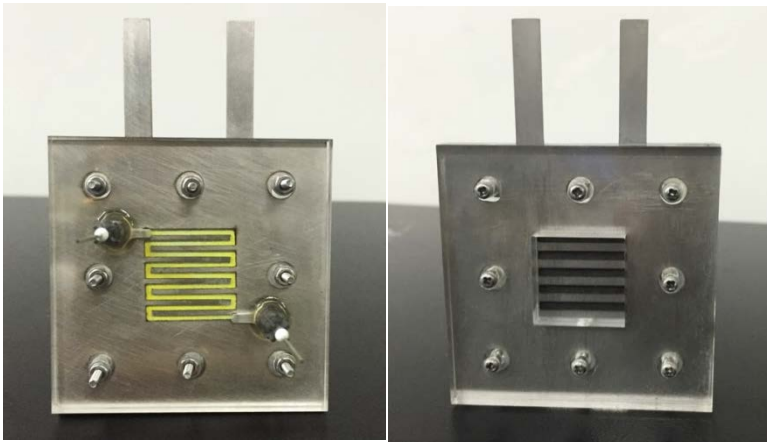

(b)

Fig. 1 (a) Schematic of the solar-responsive PEC with the MEA design, (b) Images of the fabricated PEC.

2.5 Experimental system

A data acquisition unit (34972A, Agilent, USA) and an electronic load (CT-3008, Neware Technology Ltd., China) were used to measure and record the data of the open circuit voltage, short circuit current density and polarization curves of the PEC.

A 300W xenon lamp (CELHXF300, Aulight, China) with AM 1.5G filter was used to simulate the sunlight to actuate the PEC. The light intensity was controlled by adjusting the distance between the PEC and Xenon lamp and measured by a visible-light radiometer (FZ-A, Photoelectric Instrument Factory of Beijing Normal University, China). Because this work was mainly focused on the demonstration of the feasibility of this new type of PEC, to more easily characterize the performance, ethanol was chosen as the model organics for the performance evaluation. The electrolyte (KOH or Na_2SO_4) and ethanol mixed solution was introduced into the PEC by a syringe pump (LSP04-1A, Longer Pump, China). All measurements were repeated for three times.

3. Results and discussion

3.1 Photoanode characterization

The prepared photoanode of CdS-ZnS-TiO_2/15% SBA-15 was chosen as the representative and characterized by X-ray diffraction (XRD) using an X-ray diffractometer (D8 ADVANCE, German). The result is shown in Fig. 2a. It can be seen that the crystalline diffraction peaks of CdS-ZnS-TiO_2/SBA-15 at 2θ of 25.3°, 37.8°, 38.6°, 48°, 53.9°, 55° and 62.7°were observed and identified as the anatase TiO_2. The rutile phase could also be observed at 2θ of 27.4°, 36.1° 41.3° and 54.4°, which were much weaker compared to anatase TiO_2. It is indicated that good crystalline phases were well kept during the fabrication process. Diffraction peaks corresponding to SiO_2 were not observed. The reason might be that the SiO_2 presented in the composite was in the amorphous phase. In addition, Raman spectra of

CdS-ZnS-TiO_2/SBA-15 was also characterized by LabRAM HR Evolution (HORIBA Scientific, France) and the result is shown Fig. 2b. It can be seen that there existed five scattering peaks at 146.4, 197.4, 395.4, 517.3 and 637.6 cm^{-1}, which could be assigned to TiO_2. A rather tiny peak at 477 cm^{-1} was observed, which could be assigned to SBA-15. Such weak response might be attributed to low SBA-15 mass ratio. CdS and ZnS were not clearly identified for both the XRD and Raman results mainly because of their low content.

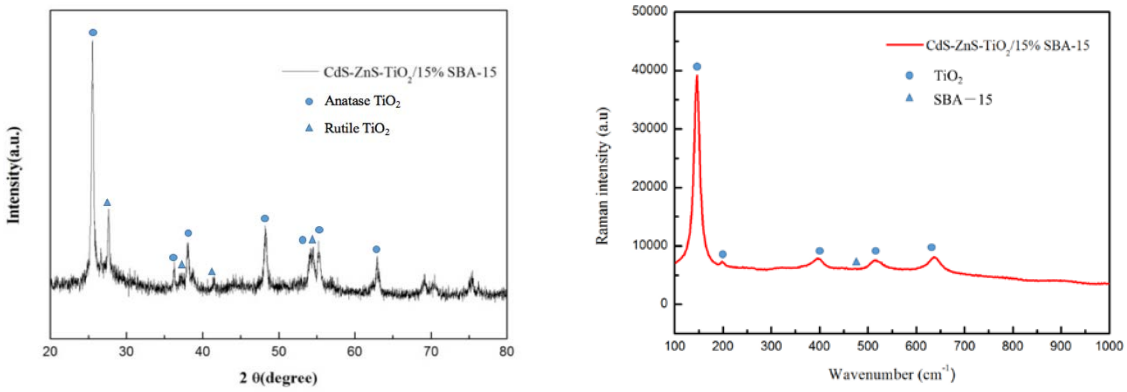

(a) (b)

Fig. 2 (a) XRD pattern and (b) Raman spectra of CdS-ZnS-TiO_2/15% SBA-15.

Furthermore, the TEM characterization was conducted (G2F20S-TWIN, Tecnai, America) and the image is given in Fig. 3a. It can be seen that after calcination at 550 ^oC, the SBA-15 particles still retained its uniform pore characteristics and were homogeneously mixed with TiO_2 particles. Furthermore, the morphologies of the prepared TiO_2/SBA-15 film with and without CdS-ZnS were also characterized by SEM using a JSM-7800F electron microscope (JEOL, Japan). The results are shown in Figs. 3b and 3c. It can be found that before the quantum-dot-sensitization by

CdS-ZnS, the TiO_2/SBA-15 film had a uniform porous structure. The TiO_2 nanoparticles were well mixed with mesoporous SBA-15. There were plentiful micro and meso pores for photon and mass transport. After 4 SILAR cycles, CdS-ZnS has been successfully deposited onto the TiO_2/SBA-15 film so that the average pore size of the CdS-ZnS-TiO_2/15% SBA-15 was reduced. More importantly, it can be found that the CdS and ZnS were well dispersed on and between TiO_2/SBA-15. Fig. 4a compares the UV-Vis diffusion reflectance spectra of TiO_2, TiO_2/SBA-15, CdS-ZnS-TiO_2/15% SBA-15. Obviously, SBA-15 had no contribution to broaden the absorption spectra to visible light, while the absorption spectra of the CdS-ZnS-TiO_2/15% SBA-15 had been extended to about 550 nm. This fact indicated that the quantum-dot-sensitization by CdS-ZnS had successfully allowed the prepared photoanode to respond to the visible light.

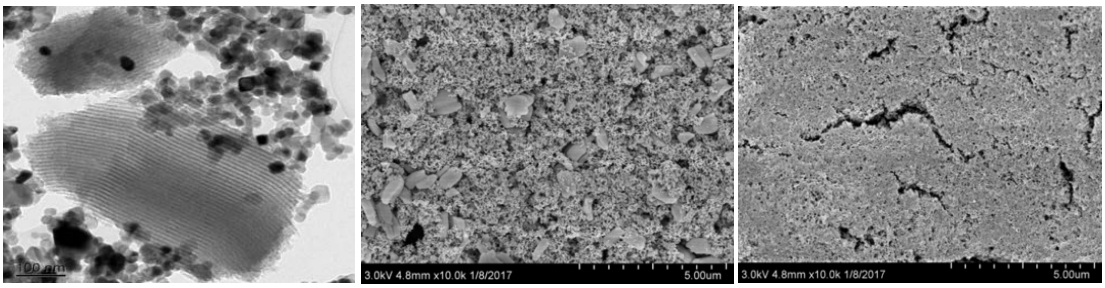

(a) (b) (c)

Fig. 3 (a) TEM image of TiO_2/SBA-15, (b) SEM image of TiO_2/SBA-15 film, and (c) SEM image of CdS-ZnS-TiO_2/15% SBA-15 film.

3.2 Photoresponse characteristics

Photoresponse behavior of the developed PEC with CdS-ZnS-TiO_2/15% SBA-15 was characterized under the light on/off mode. The light intensity was kept at 180

mW/cm^2 and the ethanol concentration was 10% by volume. The electrolyte was KOH with the concentration of 0.2 M and the liquid flow rate was 100 μL/min. The short circuit current density and open circuit voltage (OCV) were chosen as the representative current density and voltage to characterize the photoresponse behaviors. Fig. 4b shows the photoresponse of the short circuit current density to the light on/off cycle. In this work, because the illuminated area was only one half of the MEA area, the current density was calculated based on the illuminated area instead of the entire MEA area. It can be seen that once the MEA based PEC was illuminated, the current density was immediately increased to about 2.1 mA/cm^2 in a few seconds and gradually climbed to about 2.4 mA/cm^2. When the light was turned off, the current density quickly dropped to about zero. Fig. 4c shows the photoresponse of the OCV to the light on/off cycles. Similarly, when the illumination was applied, the cell voltage instantly increased to about 1.07 V. When the light was off, the voltage quickly dropped to about 0.9 V and then gradually dropped to about 0.17 V. The photoresponse behaviors of both the short circuit current density and OCV could be well reproduced, indicating that the developed PEC with the MEA design exhibits good photoresponse to the illumination.

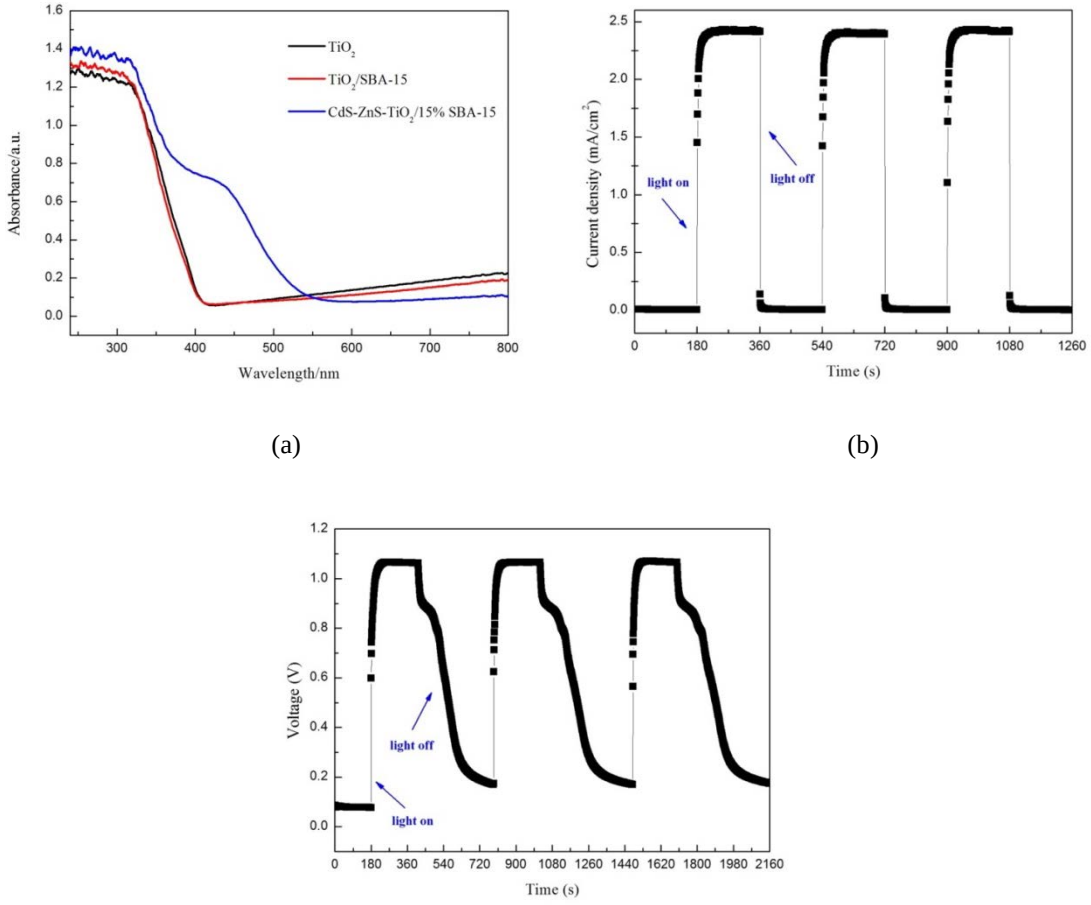

(a) (b)

(c)

Fig. 4 (a) UV-Vis absorption spectra of TiO_2, TiO_2/SBA-15 and CdS-ZnS-TiO_2/15% SBA-15, (b) the photocurrent-time curves, and (c) the photovoltage-time curves.

3.3 Typical performance

Polarization curve has been widely used to characterize the performance of the fuel cells, so that we also used the polarization curve to evaluate the performance of the developed PFC with CdS-ZnS-TiO_2/15% SBA-15. In this testing, the light intensity was 180 mW/cm^2 and ethanol concentration was 10% by volume. The KOH concentration was 0.2 M and liquid flow rate was 100 μL/min. The typical polarization curve is shown in Fig. 5a. It can be seen that when the current density

was below 1.6 mA/cm^2, the cell voltage was almost linearly decreased as the current density increased. As the current density further increased, the cell voltage started to drop quickly. The reasons leading to the reduction in the cell voltage with the increase of the current density are presented as follows. The increase of the current density means that the photoelectrochemical and electrochemical reaction rates at the photoanode and cathode are increased, which causes the overpotentials resulting from the reaction kinetics at both the electrodes are increased. Thereby, the cell voltage of the developed PEC was decreased. In the meantime, the lowered cell voltage indicated that the driving force for the transfer of the excited electrons at the photoanode to the cathode was low so that the electrons and holes were easily recombined. In this case, less hydroxyl radicals, which have strong oxidizing ability, were generated, slowing down the photoelectrochemical reaction rate and causing the overpotential of the photoanode to be further increased. This problem became more serious at low cell voltage. Therefore, the cell voltage dropped rapidly at high current densities. In addition, the increase of the current density requires more organics and OH^- ions, which results in the lowered concentrations of the organics and OH^- in the photoanode. Accordingly, the overpotential due to the concentration polarization was increased, which also caused the reduction of the cell voltage. Because of the above reasons, the cell voltage decreased with increasing the current density. With the polarization curve, the variation of the power density with the current density was also achieved. As shown, the power density firstly increased and then decreased with increasing the current density. A maximum power density of 1.09 mW/cm^2 was

obtained at the current density of 1.6 mA/cm^2, which was higher than the previous PEC with the MEA structure [28, 31]. In this work, the fill factor (FF) was also employed to characterize the performance of the PEC, which can be calculated by the following equation,

$$\mathrm{FF} = \frac{(JV)_{max}}{J_{sc}V_{oc}} \quad (1)$$

where $(JV)_{max}$ is the achieved maximum power density, J_{sc} and V_{oc} are the measured short circuit current density and open circuit voltage. Thus, the fill factor of this PEC could be calculated, which was 0.42 under these conditions. In summary, the developed PEC is able to yield favorable performance.

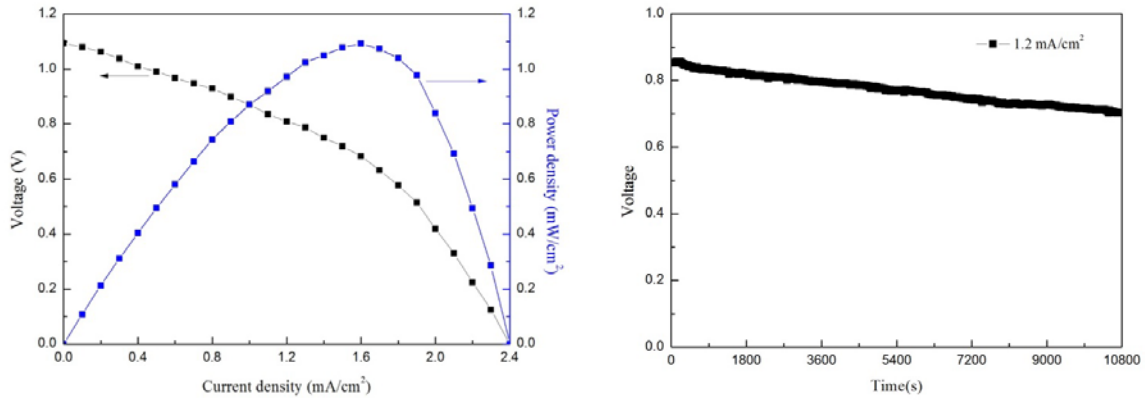

(a) (b)

Fig. 5 (a) The typical polarization curve and (b) transient discharging voltage of the developed PEC with the MEA design.

In addition, we also characterized the performance with the continuous running mode at a constant current density of 1.2 mA/cm^2 for 3 hours. In this measurement, the light intensity was 180 mW/cm^2 and the ethanol concentration was 10% by volume. The KOH concentration was 0.2 M and the liquid flow rate was kept at 100 μL/min. The variation of the cell voltage with the discharging time is shown in Fig. 5b. As seen,

the cell voltage was slightly decreased from 0.85 V to 0.71 V during the testing period. The possible reasons might be the decay of photosensitizer and the adsorption of the intermediates, which lowered the photoelectrochemical reaction rate. Although the voltage was decreased, the cell voltage was still relatively stable in the 3-h operation, which might be attributed to that the adverse effect of the photosensitizer decay and intermediates adsorption was not significant in this period.

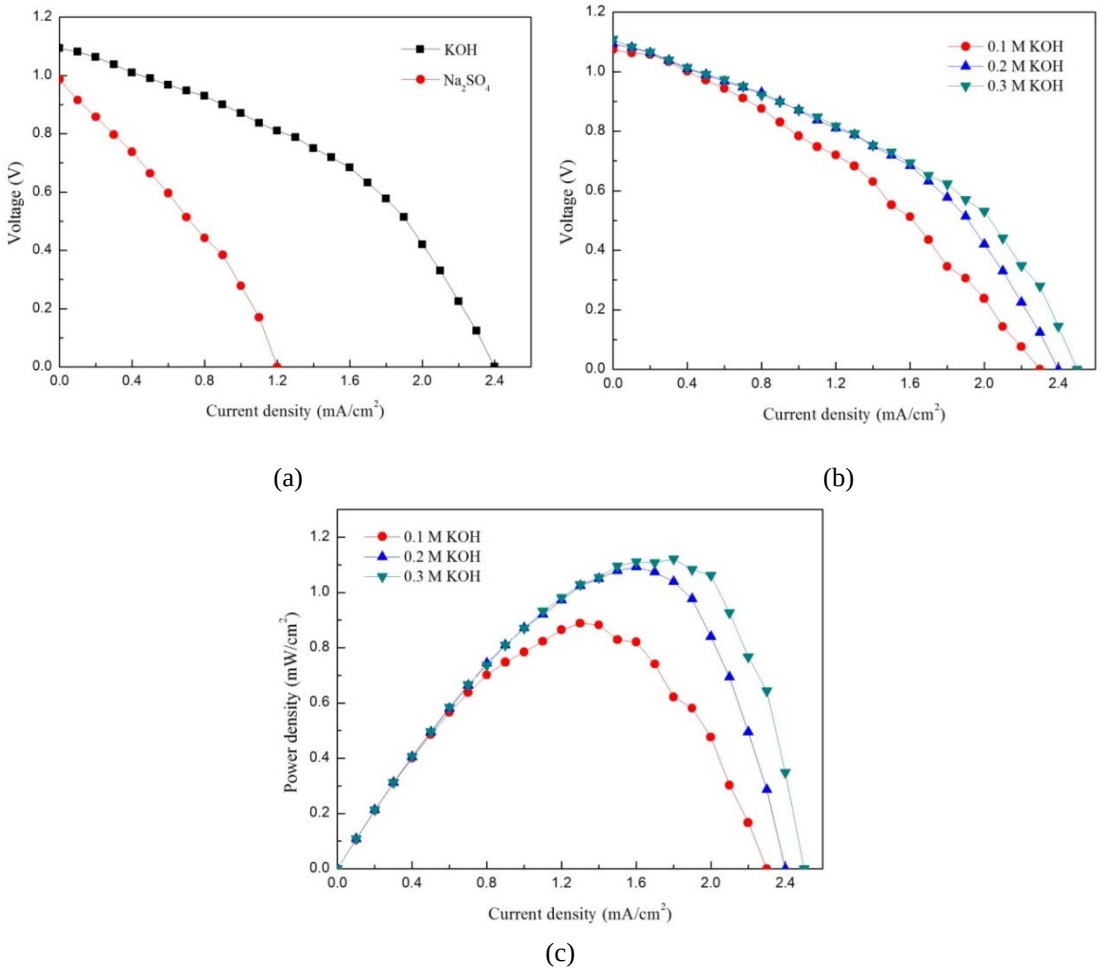

Fig. 6 (a) The polarization curve of the MEA based PEC under the alkaline and neutral conditions, (b) the variation of the performance with the KOH concentration, (c) the power density curves at different KOH concentrations.

3.4 Effect of the electrolyte condition

The electrolyte condition plays an important role in the PEC performance because the

change of the charge type will affect the reaction kinetics at both the electrodes. Generally, the electrolyte can be divided into acidic, neutral and alkaline environments. Due to the fact that the sulfide is soluble in acidic environment, only neutral and alkaline conditions were investigated. In this work, the KOH and Na_2SO_4 electrolyte solutions were chosen to represent the alkaline and neural conditions, both of which were 0.2 M. The light intensity was 180 mW/cm^2 and the ethanol concentration was 10% by volume, while the liquid flow rate was maintained at 100 μL/min. Fig. 6a shows the polarization curves of the developed PEC under the alkaline and neutral conditions. It can be seen that the performance of the PEC in the alkaline environment was much better than that in the neutral environment. The open circuit voltage and short circuit current density in the neutral environment were only 0.98 V and 1.2 mA/cm^2, respectively, which were smaller than those in the alkaline environment, 1.09 V and 2.4 mA/cm^2. These results can be attributed to the following reasons. First of all, let us look at the reactions of the photoanode and air-breathing cathode in the alkaline and neutral environments as below.

Photoanode reaction in the alkaline environment:

$$h\nu + TiO_2 = e^- + h^+ \quad (2)$$

$$C_2H_5OH + 12OH^- + 12h^+ = 2CO_2 + 9H_2O \quad (3)$$

Cathode reaction in the alkaline environment:

$$H_2O + 1/2O_2 + 2e^- = 2OH^- \quad (4)$$

Photoanode reaction in the neutral environment:

$$h\nu + TiO_2 = e^- + h^+ \quad (5)$$

$$C_2H_5OH + 3H_2O + 12h^+ = 2CO_2 + 12H^+ \quad (6)$$

Cathode reaction in the neutral environment:

$$2H^+ + 2e^- + 1/2O_2 = H_2O \quad (7)$$

As indicated by Reactions (2) and (3) in the alkaline environment, the abundant OH^- ions were supplied, which were efficient hole scavengers [32]. As a result, more photo-excited holes can be scavenged by the supplied OH^- ions to generate hydroxyl radicals, which prevented the recombination of the electron-hole pairs. Hydroxyl radicals have strong oxidizing ability, which could efficiently degrade ethanol and thereby facilitate the photoanode reactions significantly. However, in the neutral environment, the charge carriers, protons, mainly came from the photoanode reaction indicated by Reactions (5) and (6). Only a small amount of the photo-excited holes could be captured, leading to serious recombination and poor performance. Second, the alkaline condition facilitated the oxygen reduction reaction at the cathode, which also benefited for the improvement in the cell performance. Third, the charge transport between the photoanode and cathode was also different in these two cases. Although Nafion® 211 membrane intrinsically conducts cations to form the ionic current and its functional groups with negative charge hinder the OH^- migration, it has been demonstrated that highly mobile OH^- ions still experimentally contribute to nearly 70% of the ionic current and thus become the main charge carrier under the alkaline condition [33]. In this case, because a significant amount of OH^- ion has been supplied to the photoanode with the alkaline operation, the OH^- ion transport can be enhanced to reduce the internal cell resistance. Nevertheless, for the neutral

environment, the charge carrier of proton was only generated by the photoanode reaction. The proton transport between the photoanode and cathode was limited, increasing the internal cell resistance. Because of these reasons, the performance of the developed PEC in the alkaline environment was much better than that in the neutral environment.

Since the alkaline environment yielded better performance, we further studied the effect of the KOH concentration on the performance of the developed PEC, ranging from 0.1 M to 0.3 M. The results are shown in Fig. 6b. As seen, when the KOH concentration increased, the short circuit current density increased from 2.3 mA/cm^2 to 2.5 mA/cm^2, the best performance was got at the KOH concentration of 0.3 M. Besides, the OCV was slightly improved from 1.07 V to 1.09V and the maximum power density increased from 0.89 mW/cm^2 to 1.09 mW/cm^2, as shown in Fig. 6c. The improved performance can be attributed to the increase of the KOH concentration, which provides more OH^- ions to facilitate the photoelectrochemical and electrochemical reactions at both the electrodes. Meanwhile, the increased KOH concentration can reduce the ion transfer resistance through the membrane, reducing the internal cell resistance. Therefore, the performance was improved with increasing the KOH concentration in the testing range.

3.5 Effect of the SBA-15 mass ratio

Table 1 Textural properties

Sample	BET surface area (m^2/g)	Pore volume (cm^3/g)
TiO_2	52.4	-
TiO_2/15% SBA-15	120.2	0.287
TiO_2/30% SBA-15	184.8	0.437
TiO_2/45% SBA-15	256.2	0.568
TiO_2/60% SBA-15	325.3	0.731
SBA-15	565.8	1.138

As mentioned above, the addition of mesoporous SBA-15 into the photoanode is to enhance the photoanode performance. It is essential to optimize the SBA-15 mass ratio to maximize the PEC performance. For this reason, we studied the effect of the SBA-15 mass ratio on the cell performance, ranging from 15%, 30%, 45% to 60%. For comparison, a photoanode without SBA-15 (represented by CdS-ZnS-TiO_2) was also prepared with the TiO_2 loading of about 3 mg/cm^2. During the testing, the light intensity was 180 mW/cm^2 and the flow rate was kept at 100 μL/min, while the concentrations of KOH and ethanol were 0.2 M and 10% by volume, respectively. The results are shown in Fig. 7a. It can be seen that the PFC with the photoanode of CdS-ZnS-TiO_2/15% SBA-15 yielded better performance than the one without SBA-15. The short circuit current density was improved from 2.1 mA/cm^2 to 2.4 mA/cm^2 and the OCV was improved from 1.05 V to 1.09 V. The maximum power density was increased from 1.01 mW/cm^2 to 1.09 mW/cm^2. The improvement of the performance can be attributed to the addition of the SBA-15, which provided large specific surface

area and pore volume. As listed in Table 1, the BET surface area was improved from 52.4 m^2/g to 120.2 m^2/g, which allowed more CdS and ZnS to be adsorbed on the surface to facilitate the photoelectrochemical reactions. In addition, large pore volume also benefited for the reactants and photon transport, further enhancing the photoanode performance. Thereby, the performance of the PFC with the SBA-15 in the photoanode was better than the one without SBA-15. However, as the SBA-15 mass ratio was increased to 30%, although the BET surface area and pore volume could be increased, as shown in Table 1, the cell performance was decreased. The short circuit current density decreased from 2.4 mA/cm^2 to 2.3 mA/cm^2. The corresponding maximum power density decreased from 1.09 mW/cm^2 to 1.04 mW/cm^2, but which was still better than that of the photoanode without the SBA-15. This might be because the SBA-15 has poor conductivity and no photocatalytic activity towards the organics oxidation. Increasing the SBA-15 mass ratio may result in lowered electron transfer and active surface area for the photoelectrochemical reactions. As a consequence, when the SBA-15 mass ratio increased, the cell performance was reduced. However, the positive effect of the SBA-15 was still stronger than its adverse effect so that the photoanode of CdS-ZnS-TiO_2/30% SBA-15 could still yield better performance than did the photoanode of CdS-ZnS-TiO_2. As the SBA-15 mass ratio was further increased 45% and 60%, because the electrical conductivity and active surface area were greatly reduced, the cell performance was further reduced and even lower than the photoanode of CdS-ZnS-TiO_2. Correspondingly, the maximum power density was decreased to 0.68 mW/cm^2. From

these results, it can be known that the SBA-15 mass ratio of 15% exhibited the best performance in this work. Because of this, the PEC with the photoanode of CdS-ZnS-TiO_2/15% SBA-15 was used in the following parametric studies.

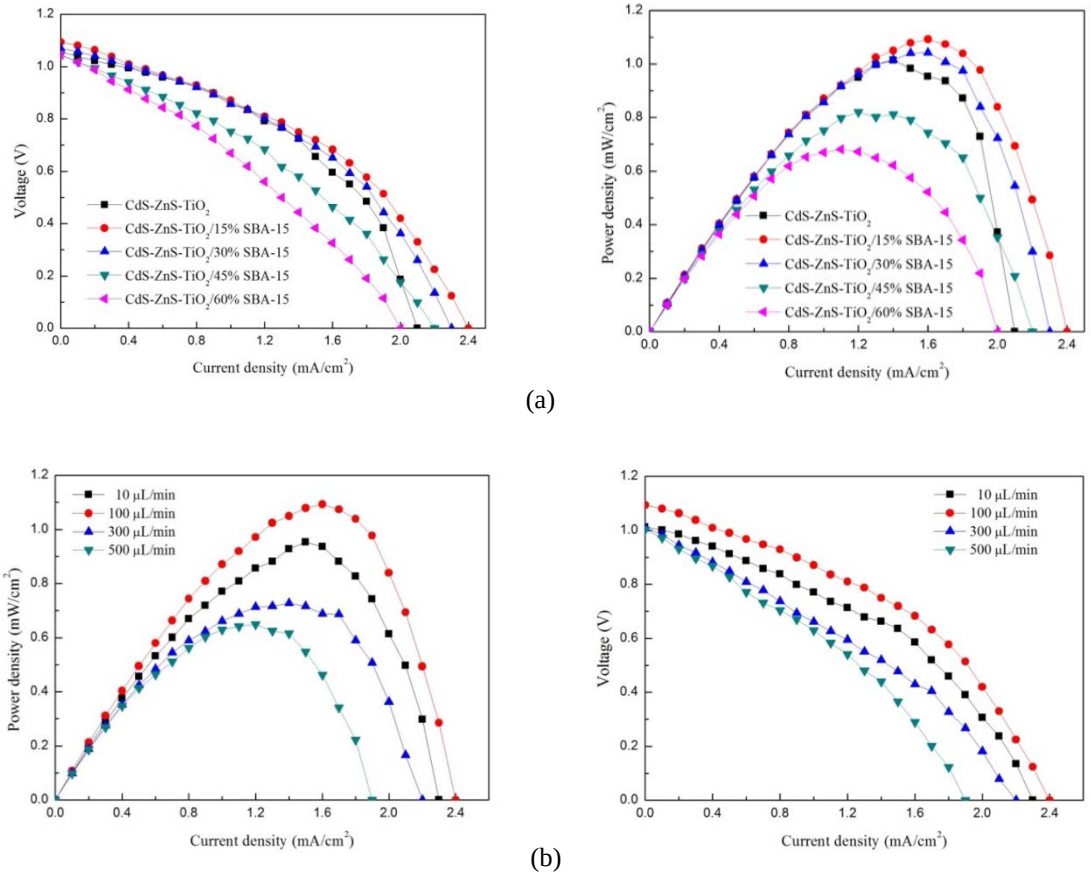

Fig. 7 Effects of (a) the SBA-15 mass ratio and (b) the liquid flow rate.

3.6 Effect of the liquid flow rate

The variation of the liquid flow rate can affect the mass transport and thus the cell performance. Hence, the effect of the liquid flow rate on the cell performance of the developed PEC was studied. To do this, the light intensity was 180 mW/cm^2, the ethanol concentration was 10% by volume and KOH concentration was 0.2 M. The flow rate ranged from 10 μL/min to 500 μL/min. Fig. 7b shows the change of the cell performance with the liquid flow rate. It can be seen that as the liquid flow rate

increased from 10 μL/min to 500 μL/min, the short circuit current density firstly increased from 2.3 mA/cm^2 to 2.4 mA/cm^2 and then decreased to 1.9 mA/cm^2. The flow rate of 100 μL/min yielded the best performance. Correspondingly, the maximum power density of 1.09 mW/cm^2 was also obtained at 100 μL/min. This might be because the 10% fuel concentration at the flow rate of 100 μL/min has provided sufficient driving force for ethanol to be transferred from the bulk liquid to the photocatalysts to meet the demand of the photoelectrochemical reactions at the photoanode. The flow rate of 10 μL/min was not enough to meet the demand of the photoanode reaction. Hence, not only the short circuit current density but also the OCV were decreased. On the other hand, although higher liquid flow rate can enhance the mass transfer to the photoanode, the organics crossover to the cathode through the membrane was also increased, resulting in a higher mixed potential at the cathode and thus lowering the cell performance, which can be evidenced by the lowered OCV. Therefore, the best cell performance was yielded at a liquid flow rate of 100 μL/min.

3.7 Effect of the organics concentration

Figure 8a shows the effect of the organics concentration on the discharging performance of the developed PEC. In this testing, the liquid flow rate was 100 μL/min, the light intensity was 180 mW/cm^2 and the KOH concentration was 0.2 M. It can be found that when the ethanol concentration was extremely low (1% by volume), the cell performance was rather poor. The reason is that critically low ethanol concentration highly limited the organics supply and thus the photoanode reaction, leading to poor performance. As the organics concentration increased to 10%,

the transport of organics was enhanced. Consequently, the cell performance was greatly improved. The short circuit current density was improved from 1.6 mA/cm^2 to 2.4 mA/cm^2 and the maximum power density was improved from 0.94 mW/cm^2 to 1.09 mW/cm^2. However, when the organics concentration was increased to 20%, the organics transport was further enhanced. The organics crossover through the membrane to the cathode was increased, resulting in a large mixed potential at the cathode and the lowered performance. As seen, the short circuit current density was dropped from 2.4 mA/cm^2 to 1.6 mA/cm^2 and the maximum power density decreased from 1.09 mW/cm^2 to 0.6 mW/cm^2. There existed an optimum fuel concentration leading to the best cell performance.

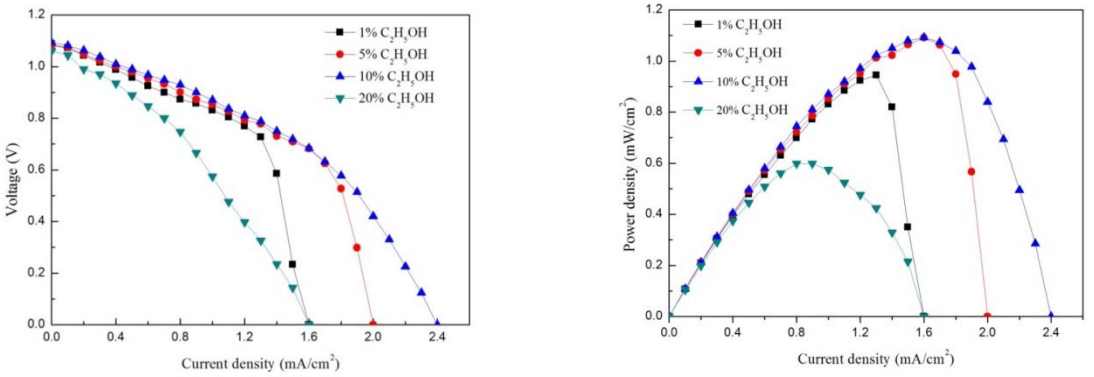

(a)

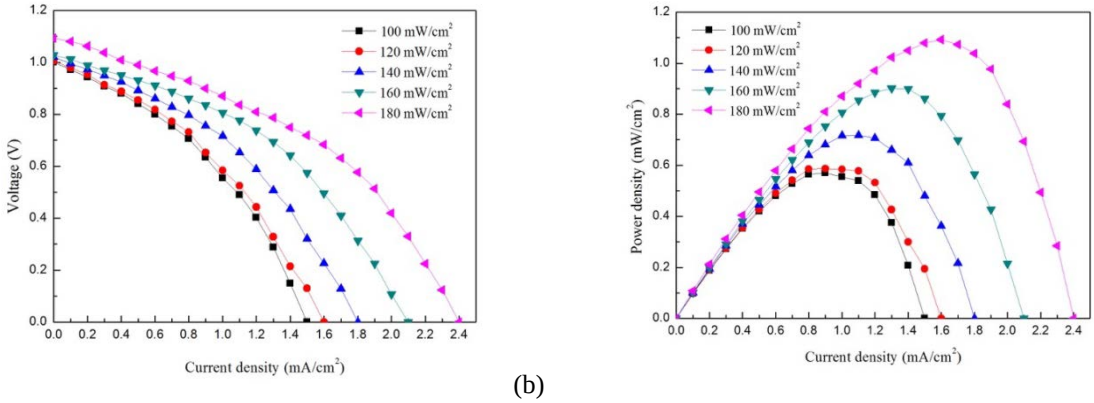

(b)

Fig. 8 Effects of (a) the organics concentration and (b) the light intensity.

3.8 Effect of the light intensity

The photoanode reaction is stimulated by the light illumination to generate the photo-excited electron-hole pairs. Therefore, the light intensity is one of the major factors affecting the PEC performance, which was also studied in this work. To do this, the ethanol concentration was kept at 10% by volume, the KOH was 0.2 M and the liquid flow rate was maintained at 100 μL/min. The light intensity ranged from 100 mW/cm^2 to 180 mW/cm^2. The results are shown in Fig. 8b. It can be seen that the increase of the light intensity led to the improvement in the cell performance. It is easy to understand that stronger light intensity produced more photo-generated electron/hole pairs, which promoted the oxidation of organics. More detailed information can be got from the polarization curves. The short circuit current density went up from 1.5 mA/cm^2 to 2.4 mA/cm^2 with the light intensity increased from 100 mW/cm^2 to 180 mW/cm^2 and the maximum power density increased from 0.57 mW/cm^2 to 1.09 mW/cm^2.

4. Conclusions

In this study, we developed a membrane electrode assembled photoelectrochemical cell with a solar-responsive mesoporous CdS-ZnS-TiO_2/SBA-15 photoanode and an air-breathing cathode for the electricity generation by simultaneously degrading organics. The design not only makes the PEC system more compact and flexible but also provides large specific surface area and pore volume for the photoelectrochemical reactions. The experimental results implied that the developed PEC exhibited good photoresponse to the illumination and its performance was

relatively stable in the 3-h operation. The photoanode with the appropriate SBA-15 mass ratio showed better performance than did the one without the SBA-15. The performance of the developed PEC was also evaluated under various operating conditions, including the electrolyte type, organics and electrolyte concentrations, liquid flow rate and light intensity. It was shown that the alkaline environment yielded better performance did the neutral environment due to the enhanced reaction kinetics at the electrodes and charge carrier transfer. Increasing the KOH concentration led to the improved performance. Too low or too high flow rate and organics concentration resulted in the low performance due to the mass transfer limitation and the organics crossover problem, respectively. There existed optimal flow rate and organics concentrations leading to the best performance. For the effect of the light intensity, the increase of the light intensity was able to improve the cell performance because more electron-hole pairs were generated. The results obtained in this study reveal that the developed PEC with the MEA design shows the promising potential for degrading organic compounds and generating electricity simultaneously by the use of solar energy.

Acknowledgments

The authors gratefully acknowledge the financial supports of the National Natural Science Foundation of China (No. 51325602, No. 51576021, No. 51276208 and No. 51506039) and the National High-Tech R&D Program of China (No. 2015AA043503).

References

[1] M. Antoniadou, P. Lianos, A photoactivated fuel cell used as an apparatus that consumes organic wastes to produce electricity, *Photochem. Photobiol. Sci.* 10 (2011) 431-435.

[2] Y.G. Adewuyi, Sonochemistry: environmental science and engineering applications, *Ind. Eng. Chem. Res*. 40 (2001) 4681-4751.

[3] R. Chen, L. Li, X. Zhu, Q. Liao, H. Wang, L. An, M.X. Zhang, A cascading gradient pore microstructured photoanode with enhanced photoelectrochemical and photocatalytic activities, *J. Catal.* 244 (2016) 411-419.

[4] X.F. He, R. Chen, X. Zhu, Q. Liao, L. An, X. Cheng, L. Li, Optofluidics based membrane microreactor for wastewater treatment by photocatalytic ozonation, *Ind. Eng. Chem. Res.* 55 (2016) 8627-8635.

[5] S.H. Bossmann, E. Oliveros, S. Göb, S. Siegwart, E.P. Dahlen, L. Payawan, M. Straub, M. Wörner, A.M. Braun, New evidence against hydroxyl radicals as reactive intermediates in the thermal and photochemically enhanced Fenton reactions, *J. Phys. Chem. A* 102 (1998) 5542-5550.

[6] P.R. Gogate, A.B. Pandit, A review of imperative technologies for wastewater treatment I: oxidation technologies at ambient conditions, *Advances in Environmental Research* 8 (2004) 501-551.

[7] M. Xia, R. Chen, X. Zhu, Q. Liao, L. An, Z.B. Wang, X.F. He, L. Jiao, A micro photocatalytic fuel cell with an air-breathing, membraneless and monolithic design, *Sci. Bull*. 61 (2016) 1699-1710.

[8] G. Chen, Electrochemical technologies in wastewater treatment, *Sep. Purif. Technol.* 38 (2004) 11-41.

[9] P. Lianos, Production of electricity and hydrogen by photocatalytic degradation of organic wastes in a photoelectrochemical cell: The concept of the Photofuelcell: A review of a re-emerging research field, *J. Hazard. Mater.* 185 (2011) 575-590.

[10] L. Li, S. Xue, R. Chen, Q. Liao, X. Zhu, Z.B. Wang, X.F. He, H. Feng, X. Cheng, Performance characteristics of a membraneless solar responsive photocatalytic fuel cell with an air-breathing cathode under different fuels and electrolytes and air conditions, *Electrochim. Acta* 182 (2015) 280-288.

[11] K. Li, H. Zhang, T. Tang, Y.L. Xu, D.W. Ying, Y.L. Wang, J.P. Jia, Optimization and application of TiO_2/Ti–Pt photo fuel cell (PFC) to effectively generate electricity and degrade organic pollutants simultaneously, *Water Res.* 62 (2014) 1-10.

[12] Y. Liu, J. Li, B. Zhou, Z. Wang, W. Cai, A TiO_2-nanotube-array-based photocatalytic fuel cell using refractory organic compounds as substrates for electricity generation, *Chem. Commun.* 47 (2011) 10314-10316.

[13] M. Antoniadou, S. Sfaelou, P. Lianos, Quantum dot sensitized titania for photo-fuel-cell and for water splitting operation in the presence of sacrificial agent, *Chem. Eng. J.* 254 (2014) 245-251.

[14] G. Williams, B. Seger, P.V. Kamat, TiO_2-graphene nanocomposites. UV-assisted photocatalytic reduction of graphene oxide, *ACS Nano* 2 (2008) 1487-1491.

[15] P. Cheng, M. Zheng, Y. Jin, Q. Huang, M. Gu, Preparation and characterization

of silica-doped titania photocatalyst through sol–gel method, *Mater. Lett.* 57 (2003) 2989-2994.

[16] M.J. López-Muñoz, V.R. Grieken, J. Aguado, J. Marugán, Role of the support on the activity of silica-supported TiO_2 photocatalysts: structure of the TiO_2/SBA-15 photocatalysts, *Catal. Today* 101 (2005) 307-314.

[17] R. Chen, X. Cheng, X. Zhu, Q. Liao, L. An, D.D. Ye, X.F. He, Z.B. Wang, High-performance optofluidic membrane microreactor with a mesoporous CdS/TiO_2/SBA-15@carbon paper composite membrane for the CO_2 photoreduction, *Chem. Eng. J.* 316 (2017) 911-918.

[18] M. Antoniadou, P. Lianos, Production of electricity by photoelectrochemical oxidation of ethanol in a photofuelcell, *Appl. Catal. B-Environ.* 99 (2010) 307-313.

[19] Q. Chen, J. Li, X. Li, K. Huang, B. Zhou, W. Cai, W. Shangguan, Visible-light responsive photocatalytic fuel cell based on WO_3/W photoanode and Cu_2O/Cu photocathode for simultaneous wastewater treatment and electricity generation, *Environ. Sci. Technol.* 46 (2012) 11451-11458.

[20] M. Kaneko, H. Ueno, R. Saito, S. Yamaguchi, Y. Fujii, J. Nemoto, UV light-activated decomposition/cleaning of concentrated biomass wastes involving also solid suspensions with remarkably high quantum efficiency, *Appl. Catal. B-Environ.* 91 (2009) 254-261.

[21] Q. Liao, L. Li, R. Chen, X. Zhu, H. Wang, D.D. Ye, X. Cheng, M.X. Zhang, Y.C. Zhou, Respective electrode potential characteristics of photocatalytic fuel cell

with visible-light responsive photoanode and air-breathing cathode, *Int. J. Hydrogen Enery.* 40 (2015) 16547-16555.

[22] M. Matsuoka, M. Kitano, S. Fukumoto, K. Iyatani, M.Takeuchi, M. Anpo, The effect of the hydrothermal treatment with aqueous NaOH solution on the photocatalytic and photoelectrochemical properties of visible light-responsive TiO_2 thin films, *Catal. Today* 132 (2008) 159-164.

[23] M. Antoniadou, P. Lianos, Photoelectrochemical oxidation of organic Substances over nanocrystalline titania: optimization of The photoelectrochemical cell, *Catal. Today* 144 (2009) 166-171.

[24] M. Antoniadou, D.I. Kondarides, D. Labou, S. Neophytides, P. Lianos, An efficient photoelectrochemical cell functioning in the presence of organic wastes *Sol. Enery. Mater. Sol. C.* 94 (2010) 592-597.

[25] L. Li, G. Wang, R Chen, X. Zhu, H. Wang, Q. Liao, Y.X. Yu, Optofluidics based micro-photocatalytic fuel cell for efficient wastewater treatment and electricity generation, *Lab Chip* 14 (2014) 3368-3375.

[26] S. Joseph, J.C. Mcclure, R. Chianelli, P. Pich, P.J. Sebastian, Conducting polymer-coated stainless steel bipolar plates for proton exchange membrane fuel cells (PEMFC), *Int. J. Hydrogen Enery.* 30 (2005) 1339-1344.

[27] P. Costamagna, S. Srinivasan, Quantum jumps in the PEMFC science and technology from the 1960s to the year 2000: Part II. engineering, technology development and application aspects, *J. Power Sources* 102 (2001) 253-269.

[28] B. Seger, P.V. Kamat, Fuel cell geared in reverse: photocatalytic hydrogen production using a TiO_2/Nafion/Pt membrane assembly with no applied bias, *J. Phys. Chem. C* 113 (2009) 18946-18952.

[29] M.K. Nazeeruddin, A. Kay, I. Rodicio, R. Humphry-Baker, E. Mueller, P. Liska, N. Vlachopoulos, M. Graetzel, Conversion of light to electricity by Cis-X2bis (2, 2'-bipyridyl-4, 4'-dicarboxylate) Ruthenium (II) charge-transfer sensitizers (X= Cl-, Br-, I-, CN-, and SCN-) on nanocrystalline titanium dioxide electrodes, *J. Am. Chem. Soc.* 115 (1993) 6382-6390.

[30] Y.F. Nicolau, Solution deposition of thin solid compound films by a successive ionic-layer adsorption and reaction process, *Applications of Surface Science* 22-23 (1985) 1061-1074.

[31] B. Seger, G.Q. Lu, L. Wang, Electrical power and hydrogen production from a photo-fuel cell using formic acid and other single-carbon organics, *J. Mater. Chem.* 22 (2012) 10709-10715.

[32] X. Cheng, R. Chen, X. Zhu, Q. Liao, L. An, D.D. Ye, X.F. He, S.Z. Li, L. Li, An optofluidic planar microreactor for photocatalytic reduction of CO_2 in alkaline environment, *Energy* 120 (2017) 276-282.

[33] L. An, T.S. Zhao, Y. Li, Q.X. Wu, Charge carriers in alkaline direct oxidation fuel cells, *Enery. Environ. Sci*. 5 (2012) 7536-7538.